ACS APPLIED MATERIALS & INTERFACES

www.acsami.org

Research Article

In Situ Coating $CsPbBr_3$ Nanocrystals with Graphdiyne to Boost the Activity and Stability of Photocatalytic CO_2 Reduction

Ke Su, Guang-Xing Dong, Wen Zhang,* Zhao-Lei Liu, Min Zhang,* and Tong-Bu Lu*

Cite This: *ACS Appl. Mater. Interfaces* 2020, 12, 50464–50471

Read Online

ACCESS | Metrics & More | Article Recommendations | Supporting Information

ABSTRACT: The instability and low inferior catalytic activity of metal-halide perovskite nanocrystals are crucial issues for promoting their practical application in the photocatalytic field. Herein, we in situ coat a thin graphdiyne (GDY) layer on $CsPbBr_3$ nanocrystals based on a facile microwave synthesis method, and employ it as a photocatalyst for CO_2 reduction. Under the protection of GDY, the $CsPbBr_3$-based photocatalyst delivers significantly improved stability in a photocatalytic system containing water concomitant with enhanced CO_2 uptake capacity. The favorable energy offset and close contact between $CsPbBr_3$ and GDY trigger swift photogenerated electron transfer from $CsPbBr_3$ to doping metal sites in GDY, boosting a remarkable improvement in the photocatalytic performance for CO_2 reduction. Without adding traditional sacrificial reductants, the cobalt-doped photocatalyst achieves a high yield of 27.7 μmol g^{-1} h^{-1} for photocatalytic CO_2 conversion to CO based on water as a desirable electron source, which is about 8 times higher than that of pristine $CsPbBr_3$ nanocrystals.

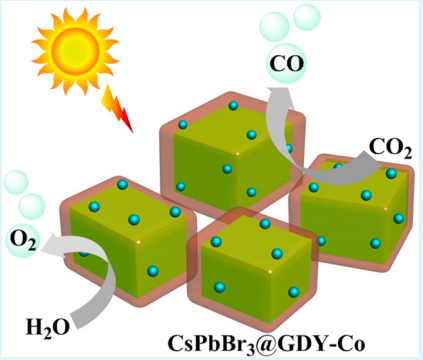

KEYWORDS: *CO_2 reduction, photocatalysis, perovskite nanocrystal, in situ coating, graphdiyne*

1. INTRODUCTION

The photocatalytic reduction of CO_2 to chemical feedstocks or fuels, using cost-effective photosynthesis systems, is an ideal strategy to reduce both the consumption of fossil fuels and the intensification of the greenhouse effect.[1−4] In this artificial photosynthesis technology, most of the designed systems separate the two halves of the reduction and oxidation reactions using expensive sacrificial electron donors or acceptors to close the catalytic cycle.[5,6] However, the reduction of CO_2 simultaneously using water as an electron donor is ultimately desired for practical application. In this regard, metal-halide perovskite (MHP) nanocrystals, which possess fascinating light-harvesting performance, excellent optoelectronic properties, and are cost-effective,[7−9] have recently been utilized to achieve photocatalytic reduction of CO_2 concurrent with desirable water oxidation,[10−15] demonstrating great potential in the field of practical artificial photosynthesis.[16−19] However, there are two problems in MHP nanocrystal based photocatalytic systems that need to be solved urgently for its successful application in artificial photosynthesis. First, the ionic nature of MHP nanocrystals severely reduces their stability in reaction systems containing plenty of water.[20−22] Second, the lack of effective catalytic sites and inferior charge separation limit them for high photocatalytic performance.[13,23−28] To date, these obstacles still require facile and effective solutions.

In order to settle these open questions, in this contribution, we in situ coat a thin graphdiyne (GDY) layer, a new member of the carbon family,[29] onto the surface of $CsPbBr_3$ nanocrystals (coded as $CsPbBr_3$@GDY) based on a facile microwave synthesis method (Scheme 1),[30] and employ it as a

Scheme 1. Illustration of the Synthesis of Cobalt Doped $CsPbBr_3$@GDY and Its Photoredox Reactions

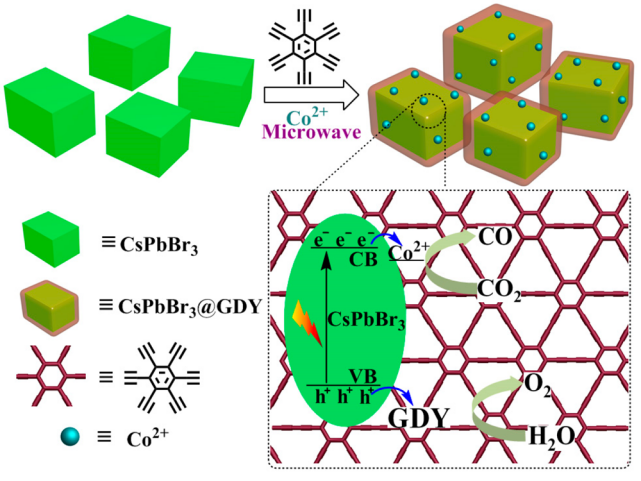

Received: August 17, 2020
Accepted: October 16, 2020
Published: October 29, 2020

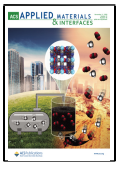

https://dx.doi.org/10.1021/acsami.0c14826
ACS Appl. Mater. Interfaces 2020, 12, 50464–50471

compatible platform for the decoration of metal ions as active sites for photocatalytic CO_2 reduction. Our strategy is mainly based on the following important considerations: (1) Coating the all-carbon material GDY on the surface of nanocrystals can improve the structural and interfacial stabilities of the nanocrystals.[31] (2) The sp-hybridized carbon atoms and triangular cavities in the GDY facilitate the metal atom doping to increase the active sites for photocatalytic reaction.[32,33] (3) The favorable energy offset and close contact between $CsPbBr_3$ and GDY can trigger swift photogenerated carrier transfer between $CsPbBr_3$ and GDY, thus boosting the improvement of the photoinduced charge separation efficiency of $CsPbBr_3$ and the catalytic activity of the composite photocatalyst. As expected, the $CsPbBr_3$@GDY composite photocatalysts deliver significantly improved stability in a photocatalytic system containing water. Using water as an electron source, a high yield of 27.7 μmol g^{-1} h^{-1} for visible-light-driven CO_2 conversion to CO has been achieved by doping cobalt ions.

2. RESULTS AND DISCUSSION

2.1. Synthesis and Characterization of $CsPbBr_3$@GDY. The $CsPbBr_3$@GDY nanocomposite was prepared with a two-step synthetic method, and the detailed procedures are described in the Experimental Section. Briefly, $CsPbBr_3$ nanocrystals were first prepared via the solution phase synthesis strategy according to a previous report (see details in the Supporting Information, SI).[15] Then the as-prepared $CsPbBr_3$ nanocrystals, acting as a growth substrate, were mixed with different amounts of hexaethynylbenzene monomer in a microwave reactor and heated for 10 min (Scheme 1). Depending on the amount of hexaethynylbenzene monomer, the obtained samples were labeled as $CsPbBr_3$@$GDY_{0.1}$, $CsPbBr_3$@$GDY_{0.3}$, and $CsPbBr_3$@$GDY_{0.5}$, respectively. For comparison, pristine GDY was also prepared under the same conditions in the absence of $CsPbBr_3$ nanocrystals (Figure S1).[30] Transmission electron microscopy (TEM) measurements (Figure 1a and 1b) show that both $CsPbBr_3$ and $CsPbBr_3$@GDY present as cubic nanostructures with a particle size of 10−20 nm. For the $CsPbBr_3$@$GDY_{0.3}$ sample, the GDY layer wrapped tightly around the surface of the $CsPbBr_3$ nanocrystal and formed a shell structure with a thickness of 1.9 nm (inset of Figure 1b). In constrast, the HRTEM image of pure $CsPbBr_3$ (Figure S2) shows relatively narrower and more ambiguous edges around the $CsPbBr_3$ nanocrystal, which may result from the adhesion of oleic acid and oleylamine residuals on the surface of $CsPbBr_3$ (Figure S3). Powder X-ray diffraction (XRD) measurements (Figure 1c) show that $CsPbBr_3$@$GDY_{0.1}$, $CsPbBr_3$@$GDY_{0.3}$, and $CsPbBr_3$@$GDY_{0.5}$ have the same crystal forms as individual $CsPbBr_3$, characteristic of a cubic phase (JCPDS 00-054-0752), indicating that the crystal structure of $CsPbBr_3$ is maintained during the process of in situ coating. The Raman spectra of $CsPbBr_3$@$GDY_{0.1}$, $CsPbBr_3$@$GDY_{0.3}$, and $CsPbBr_3$@$GDY_{0.5}$ (Figure S4) show two characteristic peaks at 1930.6 and 2102.8 cm^{-1}, which can be ascribed to the typical signals of acetylene bonds and conjugated diyne chains, evidencing the successful synthesis of GDY on $CsPbBr_3$ nanocrystals.[29,34] Furthermore, X-ray photoelectron spectroscopy (XPS) measurements were conducted to illustrate the chemical bonds in $CsPbBr_3$@$GDY_{0.3}$. The C 1s spectrum of $CsPbBr_3$@$GDY_{0.3}$ (Figure 1d) shows that the carbon species of $CsPbBr_3$@$GDY_{0.3}$ can be deconvoluted into six peaks, including C−C(sp^3), C═C (sp^2), C≡C(sp), C−N, C−O, and C═O.[35,36] The calculated integral ratio of sp- and sp^2-hybridized carbon is close to 2, further confirming the successful coating of GDY onto $CsPbBr_3$ nanocrystals.[29,30]

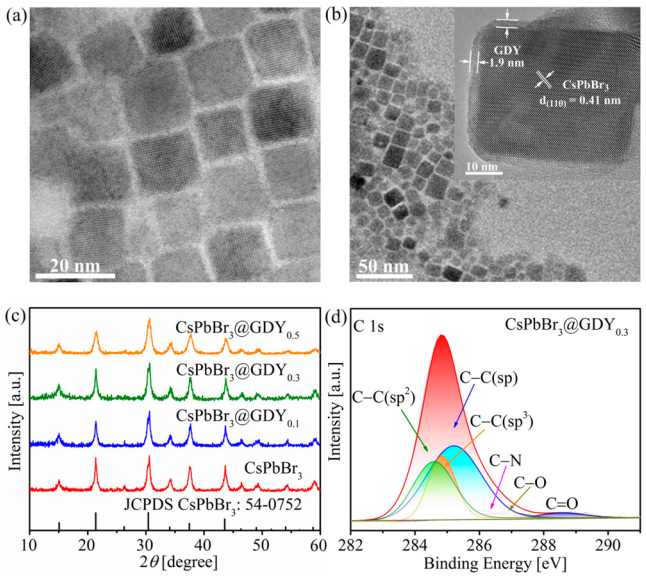

Figure 1. TEM images of (a) $CsPbBr_3$ and (b) $CsPbBr_3$@$GDY_{0.3}$, (inset: HRTEM image). (c) XRD patterns of $CsPbBr_3$ and $CsPbBr_3$@$GDY_{0.1-0.5}$. (d) XPS spectra of C 1s for $CsPbBr_3$@$GDY_{0.3}$.

2.2. Photocatalytic Reduction of CO_2. The coating effect of GDY on the photocatalytic performance of $CsPbBr_3$ for CO_2 reduction was assessed by adjusting the amount of introduced hexaethynylbenzene monomer during the microwave synthesis process. Specifically, the photoreactions were carried out in a CO_2-saturated solution of acetonitrile with H_2O as the electron donor. A xenon lamp equipped with a 400 nm filter was used as the illuminant, with a light intensity of 100 mW cm^{-2}. The results of gas chromatographic measurements and ^{13}C nuclear magnetic resonance spectroscopy (Figure 2a, Figure S5 and Table S1) imply that the major product of CO_2 reduction is CO for all the evaluated photocatalysts, and the in situ coating of GDY can significantly enhance the photocatalytic activity of $CsPbBr_3$. Herein, the adverse production of CH_4 may result from the competing desorption of CO, which could act as an intermediate for the conversion of CH_4.[37] Besides, increasing the content of GDY results in a volcanic tendency of CO production. The evolution of CO reaches an optimal value of 10.2 μmol g^{-1} h^{-1} when $CsPbBr_3$@$GDY_{0.3}$ is used as photocatalyst, 3.1 times that of pure $CsPbBr_3$ (3.3 μmol g^{-1} h^{-1}). The activity degradation of $CsPbBr_3$@$GDY_{0.5}$ may originate from the significant opacity and severe light scattering caused by excessive GDY, suggesting that an appropriate amount of GDY coating is critical to improve the photocatalytic performance of $CsPbBr_3$. It is worth noting that the amount of surface oleic acid and oleylamine residuals could also effect the composition between $CsPbBr_3$ and GDY. Sufficient washing times of $CsPbBr_3$ are significant to balance the carrier transport between $CsPbBr_3$ and GDY as well as the stability of the $CsPbBr_3$@$GDY_{0.3}$ composite (Figure S6). For comparison, the photocatalytic activity of the physical mixture of $CsPbBr_3$ and GDY was also tested (2.1 μmol g^{-1} h^{-1}); however, no enhancement was observed compared with pure $CsPbBr_3$, indicating the

https://dx.doi.org/10.1021/acsami.0c14826
ACS Appl. Mater. Interfaces 2020, 12, 50464−50471

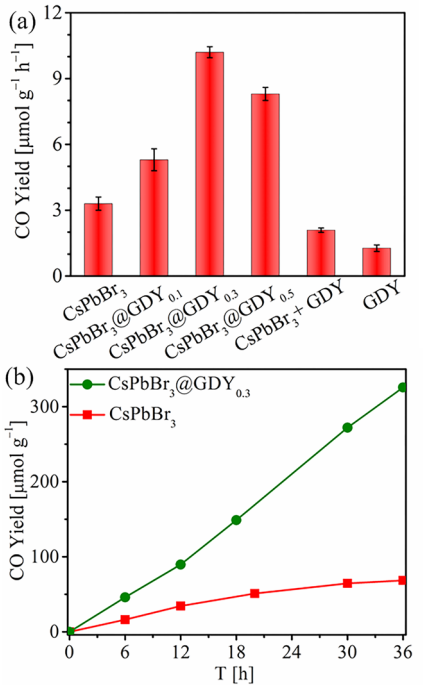

Figure 2. (a) The yields of CO productions from photocatalytic CO_2 reduction using $CsPbBr_3$, $CsPbBr_3$@$GDY_{0.1-0.5}$, a mixture of $CsPbBr_3$ and GDY, and GDY as photocatalysts. (b) The tracking of CO production over time.

remarkable benefit of close contact between $CsPbBr_3$ and GDY for the separation of photogenerated carriers. For pristine GDY, which displays a natural band gap and has been applied as a photoactive material in many reports,[38−40] trace amounts of CO were detected (1.2 μmol g^{-1} h^{-1}), suggesting that GDY itself was almost inactive for photoreduction of CO_2 in this system. Furthermore, the impact of GDY coating on the stability of $CsPbBr_3$ was also investigated in the photocatalytic experiment. As shown in Figure 2b, there is no observable decrease of CO evolution for $CsPbBr_3$@$GDY_{0.3}$ after 36 h of photocatalytic reaction. In contrast, the photocatalytic activity of pure $CsPbBr_3$ shows an obvious stagnation after 12 h illumination. In addition, the XRD and Raman spectra measurements (Figures S7 and S8) indicated that there are no significant changes in crystal structure and Raman signals for $CsPbBr_3$@$GDY_{0.3}$ before and after photoreaction, demonstrating the stability of $CsPbBr_3$@$GDY_{0.3}$ during the photoreaction. While for $CsPbBr_3$, some new peaks related to the crystalline phase of $CsPb_2Br_5$ are observed after photoreaction (Figure S9), indicating that the stability of $CsPbBr_3$ is relatively weak compared with $CsPbBr_3$@GDY. These comparative results suggest that the coating of GDY can improve the activity and stability of $CsPbBr_3$ nanocrystals photocatalysts concurrently.

To verify the origin of CO product, a $^{13}CO_2$ isotope labeling experiment (Figure S10) was conducted. The gas chromatography−mass spectrometry (GC−MS) measurement shows that an m/z = 29 corresponding to ^{13}CO was clearly detected, indicating that CO is the product of the CO_2 reduction. Additionally, increasing O_2 was also detected in the gas system besides the CO product during photoreactions. To verify that O_2 originates from the photo-oxidation of H_2O, isotopic experiment with $H_2{}^{18}O$ was conducted. The signal at m/z = 36 corresponding to $^{18}O_2$ was detected by GC−MS measurement (Figure S11), demonstrating that H_2O is the electron donor for the annihilation of photogenerated holes in $CsPbBr_3$@$GDY_{0.3}$ catalyst.

2.3. Coating Effect of GDY. To better understand the origin of the photocatalytic enhancement induced by the in situ coating of GDY on the $CsPbBr_3$ surface, the electronic band structures of GDY and $CsPbBr_3$ were first measured, which have a crucial influence on the interfacial charge transfer between GDY and $CsPbBr_3$. As shown in Figure S12, the band gap of $CsPbBr_3$ can be determined via the UV−vis spectrum of $CsPbBr_3$, which is 2.37 eV. The conduction band (CB) potentials of $CsPbBr_3$ and GDY derived from the Mott−Schottky plots (Figure S13) are −1.07 and −0.98 V versus the normal hydrogen electrode (NHE), respectively. Furthermore, the valence band (VB) spectra of XPS suggest that the VB potential of GDY is located 0.3 eV above $CsPbBr_3$ (Figure S14). Accordingly, the relative energy-band positions of $CsPbBr_3$ and GDY can be diagrammed in Figure 3a. It can

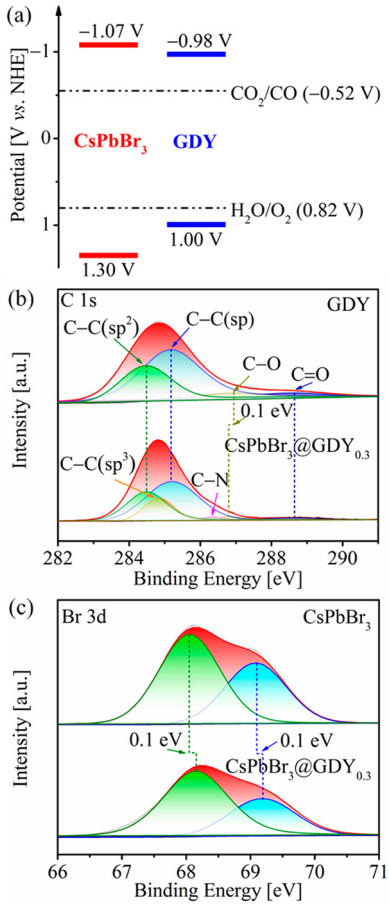

Figure 3. (a) Energy band structures of $CsPbBr_3$ and GDY. (b) XPS spectra of C 1s for GDY and $CsPbBr_3$@$GDY_{0.3}$. (c) XPS spectra of Br 3d for $CsPbBr_3$ and $CsPbBr_3$@$GDY_{0.3}$.

be noted that both of the photogenerated electrons in the CBs of $CsPbBr_3$ and GDY are energetically competent to trigger the reduction of CO_2 to CO; however, owing to the poor separation efficiency of photogenerated carriers, pristine GDY shows almost no detectable photoactivity toward CO_2 reduction (Figure 2a) or other reaction.[41] Besides, as shown in Figure 3a, the photogenerated holes of $CsPbBr_3$ can transfer

https://dx.doi.org/10.1021/acsami.0c14826
ACS Appl. Mater. Interfaces 2020, 12, 50464−50471

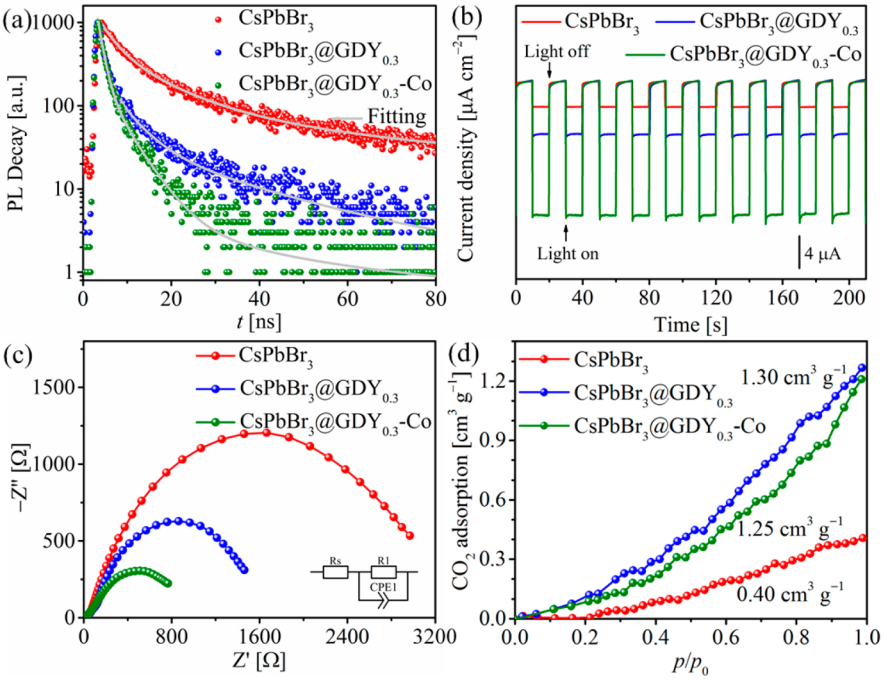

Figure 4. (a) PL decay traces, (b) $I-t$ curves, and (c) EIS spectra of $CsPbBr_3$, $CsPbBr_3$@$GDY_{0.3}$, and $CsPbBr_3$@$GDY_{0.3}$-Co under light irradiation. (d) The adsorption curves of CO_2 for $CsPbBr_3$, $CsPbBr_3$@$GDY_{0.3}$, and $CsPbBr_3$@$GDY_{0.3}$-Co.

to the VB of GDY, which could improve the separation efficiency of the photogenerated charges in $CsPbBr_3$.

XPS measurements were further carried out to analyze the interface interaction behaviors between $CsPbBr_3$ and GDY. As presented in Figure 3b, the subpeak corresponding to C−O in the C 1s peak of $CsPbBr_3$@$GDY_{0.3}$ shows a perceptible shift to low energy (by ∼0.1 eV) compared to that of pristine GDY. Meanwhile, there are distinct positive shifts of Br $3d_{5/2}$ and Br $3d_{3/2}$ peaks (∼0.1 eV) in $CsPbBr_3$@$GDY_{0.3}$ with respect to that in pristine $CsPbBr_3$ (Figure 3c). In addition, the binding energies of Cs 3d (Figure S15) and Pb 4f (Figure S16) in $CsPbBr_3$@$GDY_{0.3}$ also feature perceivable positive shifts in comparison with those in pure $CsPbBr_3$ nanocrystals. These shifts of binding energies indicate the occurrence of strong interfacial electronic coupling between $CsPbBr_3$ and GDY. The orientation of binding energy suggests that the electrons in the surface of $CsPbBr_3$ tend to migrate to GDY, resulting in a built-in electric field at the interface of $CsPbBr_3$@$GDY_{0.3}$, pointing from $CsPbBr_3$ to GDY. This built-in electric field can facilitate the photogenerated holes transfer from $CsPbBr_3$ to GDY, suggesting that the photogenerated electrons and holes of $CsPbBr_3$ could be separated efficiently.

The time-correlated single photon counting (TCSPC) technique was further utilized to study the detailed dynamics of photogenerated charge transfer between $CsPbBr_3$ and GDY. As presented in Figure 4a, the time-correlated photoluminescence (PL) decay traces could be well fitted with a three-exponential function to determine the averaged lifetime of PL decays (Table S2). The PL decay trace of pure $CsPbBr_3$ (red symbols in Figure 4a) featuring an averaged lifetime of 28.10 ns could be ascribed to the deactivation of photogenerated excitons in the $CsPbBr_3$ nanocrystals through radiative and nonradiative modes. Coating GDY onto $CsPbBr_3$ results in a significantly accelerated PL decay (blue symbols). The corresponding averaged PL lifetime of $CsPbBr_3$@$GDY_{0.3}$ is 9.48 ns (Table S2), which is noticeably shorter than that of pristine $CsPbBr_3$ (28.10 ns, Table S2), demonstrating the occurrence of efficient carrier transfer between $CsPbBr_3$ and GDY, owing to their strong interfacial interaction and favorable energy-offset. In addition, photocurrent response and electrochemical impedance spectroscopy (EIS) experiments were conducted to illustrate the benefit of GDY on the charge separation/transfer between $CsPbBr_3$ and GDY. As shown in Figure 4b, the photocurrent density of $CsPbBr_3$@$GDY_{0.3}$ is notably larger than that of $CsPbBr_3$, indicating a more efficient photogenerated carrier separation of $CsPbBr_3$@$GDY_{0.3}$ in comparison with pristine $CsPbBr_3$. The EIS of $CsPbBr_3$@$GDY_{0.3}$ with a smaller arc diameter (Figure 4c) further demonstrates a higher electron mobility of $CsPbBr_3$@$GDY_{0.3}$ compared to pure $CsPbBr_3$. These results once again confirm the beneficial impact of GDY on the interfacial carrier separation/transfer.

Apart from the separation efficiency of photogenerated carriers, the concentration of CO_2 on a photocatalyst also has an important influence on the photocatalytic activity. Thereby, the influence of coating GDY on the CO_2 uptake ability was further investigated by recording the CO_2 adsorption curves of $CsPbBr_3$ and $CsPbBr_3$@$GDY_{0.3}$. As depicted in Figure 4d, $CsPbBr_3$@$GDY_{0.3}$ has an adsorption capacity of 1.3 cm^3 g^{-1} toward CO_2, which is 3.2 times higher than that of $CsPbBr_3$, suggesting that the coating of GDY can enrich CO_2 to the surface of the catalyst. The remarkable improvement in CO_2 adsorption capacity may be ascribed to the unique structure of GDY's characteristic carbon−carbon triple bonds with delocalized electrons and abundant distributed pores, which has been demonstrated to be beneficial for the CO_2 adsorption.[42,43] Overall, coating GDY onto the surface of $CsPbBr_3$ can bring forth an enhanced gathering ability toward CO_2 and improved separation efficiency of photogenerated carriers, which jointly contribute to the aforementioned higher photocatalytic activity of $CsPbBr_3$@$GDY_{0.3}$ compared to pure $CsPbBr_3$.

https://dx.doi.org/10.1021/acsami.0c14826
ACS Appl. Mater. Interfaces 2020, 12, 50464−50471

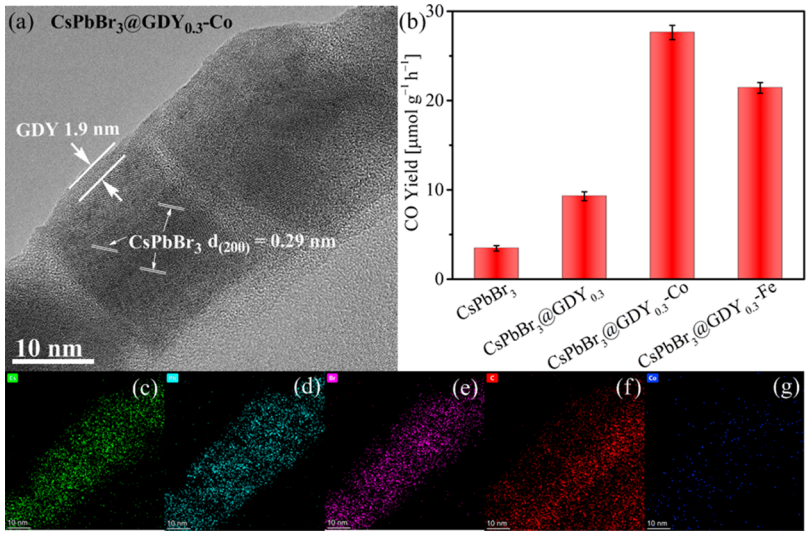

Figure 5. (a) HRTEM image for $CsPbBr_3$@$GDY_{0.3}$-Co; (b) photocatalytic CO production yields of $CsPbBr_3$, $CsPbBr_3$@$GDY_{0.3}$, $CsPbBr_3$@$GDY_{0.3}$-Co, and $CsPbBr_3$@$GDY_{0.3}$-Fe; and (c–g) elemental mapping images (Cs, Pb, Br, C, and Co) of $CsPbBr_3$@$GDY_{0.3}$-Co.

2.4. Doping of Co(II) on $CsPbBr_3$@GDY. As GDY contains abundant sp-hybridized carbons, which can serve as a favorable substrate for the deposition of metal species,[44−46] Co(II) ions were chosen as catalytic sites to trap the photoexcited electrons and transfer them to reduce CO_2. The synthetic process for cobalt-doped $CsPbBr_3$@$GDY_{0.3}$ ($CsPbBr_3$@$GDY_{0.3}$-Co) is similar to that of $CsPbBr_3$@$GDY_{0.3}$, except that $CoBr_2$ was added to the mixed solution of $CsPbBr_3$ nanocrystals and hexaethynylbenzene monomer during microwave synthesis (see Experimental Section). The decoration of Co(II) (Table S3, 1.56 wt %) on $CsPbBr_3$@$GDY_{0.3}$ was characterized through XPS, TEM, and element mapping measurements. As shown in Figure S17, the binding energy of Co $2p_{1/2}$ at 780.9 eV demonstrates that the cobalt in $CsPbBr_3$@$GDY_{0.3}$-Co presents as Co^{2+}.[47] Herein, the presence of Co is thought to be supported by GDY in a monodisperse form, as the doping of Co in $CsPbBr_3$@$GDY_{0.3}$-Co is through the post synthesis method, in which the prepared $CsPbBr_3$ nanocrystals were used as a substrate to support GDY and Co. Thus, it is difficult to dope cobalt ions into the crystal lattice of $CsPbBr_3$ nanocrystal through this method. Besides, the doping of Co has no influence on the crystalline structure of $CsPbBr_3$ (Figure S18) and the UV−vis spectra (Figure S19) of $CsPbBr_3$@$GDY_{0.3}$, and the HRTEM image of $CsPbBr_3$@$GDY_{0.3}$-Co (Figure 5a) shows no nanoparticles other than $CsPbBr_3$ nanocrystals. All these results suggest that the presence of Co in $CsPbBr_3$@$GDY_{0.3}$-Co is supported by GDY in a monodisperse form. As the reduction potential of Co^{2+}/Co is around −0.76 V vs NHE,[13] it is thermodynamically feasible to trap the photoexcited electrons in $CsPbBr_3$@$GDY_{0.3}$-Co and act as active sites to drive the conversion of CO_2-to-CO (−0.52 V vs NHE). Besides, the binding energy of Co 2p in $CsPbBr_3$@$GDY_{0.3}$-Co shows an apparent negative shift in comparison with $CoBr_2$; combined with the significant positive shifts of binding energies for Cs 3d, Pb 4f, Br 3d, and C 1s in $CsPbBr_3$@$GDY_{0.3}$-Co with respect to those in $CsPbBr_3$@$GDY_{0.3}$ (Figures S20−23), the strong binding behavior of Co^{2+} on $CsPbBr_3$@$GDY_{0.3}$ is evidenced, and the photoexcited electrons in $CsPbBr_3$@$GDY_{0.3}$ are conducive to transfer to Co^{2+} sites. Furthermore, TEM (Figure 5a) and elemental mappings (Figure 5c–g) indicate that Co cations are uniformly dispersed in $CsPbBr_3$@$GDY_{0.3}$-Co. Besides, $CsPbBr_3$@$GDY_{0.3}$-Co shows an adsorption capacity of 1.25 cm^3 g^{-1} toward CO_2 (Figure 4d), which is close to that of $CsPbBr_3$@$GDY_{0.3}$, suggesting that the coating of GDY was the main reason to enrich CO_2 in the photocatalytic system.

The photocatalytic activity of $CsPbBr_3$@$GDY_{0.3}$-Co was investigated in the same reaction conditions as $CsPbBr_3$ and $CsPbBr_3$@$GDY_{0.3}$. The results in Figure 5b show that, without adding extra sacrificial reductants, the cobalt-doped $CsPbBr_3$@$GDY_{0.3}$ exhibits significant improvement in photocatalytic reduction of CO_2 to CO (27.7 μmol g^{-1} h^{-1}), 8 times higher than that of pristine $CsPbBr_3$ (3.3 μmol g^{-1} h^{-1}), further indicating the beneficial transfer of photogenerated electrons from $CsPbBr_3$@$GDY_{0.3}$ to doping cobalt sites. In addition, the transient PL, photocurrent response, and EIS measurements (Figure 4a–c) concurrently indicated that the doping of cobalt sites can further improve the separation of photogenerated carriers and increase the number of active sites for CO_2 reduction. Furthermore, the decoration of Fe on $CsPbBr_3$@$GDY_{0.3}$ (coded as $CsPbBr_3$@$GDY_{0.3}$-Fe) can also improve the activity of $CsPbBr_3$@$GDY_{0.3}$ from 10.2 μmol g^{-1} h^{-1} to 21.5 μmol g^{-1} h^{-1} (Figure 5b), demonstrating that the coating of GDY can act as a compatible platform for decorating a variety of active sites for other catalytic reactions. To investigate the stability of $CsPbBr_3$@$GDY_{0.3}$-Co in the photoreaction system, the cycle experiments of $CsPbBr_3$@$GDY_{0.3}$-Co and $CsPbBr_3$ have been conducted. The results in Figure S24 show that there is 11% deactivation of CO production activity after four continuous cycles of the photoreactions for $CsPbBr_3$@$GDY_{0.3}$-Co. In contrast, the photocatalytic performance of $CsPbBr_3$ decreased by 58% after the same recycling experiments, demonstrating that $CsPbBr_3$@$GDY_{0.3}$-Co is more stable in the photoreaction system than $CsPbBr_3$. In addition, the varieties of structure, morphology, and electronic structure after cycles for $CsPbBr_3$@$GDY_{0.3}$-Co were also studied. As shown in Figures S25−S27, the TEM image, XRD, and Raman spectra of $CsPbBr_3$@$GDY_{0.3}$-Co demonstrate no significant morphologic and electronic structure changes after photocatalytic reactions. These results indicate that $CsPbBr_3$@$GDY_{0.3}$-Co was relatively stable compared to pure $CsPbBr_3$ during photocatalytic CO evolution, demonstrating that the coating of GDY

https://dx.doi.org/10.1021/acsami.0c14826
ACS Appl. Mater. Interfaces 2020, 12, 50464−50471

could improve the stability and the photocatalytic performance of $CsPbBr_3$-based catalysts. Furthermore, when the photocatalytic reactions were carried out on a large scale (with 21 mg catalyst), the conversion activities of CO_2-to-CO for $CsPbBr_3$@$GDY_{0.3}$ (9.8 μmol g^{-1} h^{-1}) and $CsPbBr_3$@$GDY_{0.3}$-Co (25.0 μmol g^{-1} h^{-1}) are better than pure $CsPbBr_3$ (3.0 μmol g^{-1} h^{-1}) (Figure S28). The highest CO evolution activity was also achieved by $CsPbBr_3$@$GDY_{0.3}$-Co, which is 8.3 times higher than that of pure $CsPbBr_3$, indicating that the as-prepared $CsPbBr_3$@$GDY_{0.3}$-Co photocatalyst possesses superior performance for photocatalytic reduction of CO_2 even at large scale. Finally, the proposed reaction pathways for the reduction of CO_2 to CO and the oxidation of H_2O were illustrated in Figure S29 referring to previous reports.[48,49] For the reduction of CO_2, the Co^{2+} ions on $CsPbBr_3$@$GDY_{0.3}$-Co could act as the active site. With the supply of photoexcited electron (e^-) on $CsPbBr_3$@$GDY_{0.3}$, the proton-coupled electron transfer (PCET) process and the cleavage of the C−OH bond within ($CsPbBr_3$@$GDY_{0.3}$-Co)···COOH can take place to generate CO. For the oxidation of H_2O, the ($CsPbBr_3$@$GDY_{0.3}$-Co)=O species can be formed after subtraction of the electrons, by photoexcited holes (h^+), and protons. Then ($CsPbBr_3$@$GDY_{0.3}$-Co)=O could undergo the O−O coupling with water to generate ($CsPbBr_3$@$GDY_{0.3}$-Co)−O−OH, and produces oxygen through a reductive elimination step to regenerate the $CsPbBr_3$@$GDY_{0.3}$-Co.

3. CONCLUSIONS

In summary, we have successfully synthesized $CsPbBr_3$@GDY composite photocatalyst by in situ coating a 1.9 nm-thick GDY layer onto $CsPbBr_3$ nanocrystals. The thin GDY layer can not only enhance the stability of $CsPbBr_3$ in the water-containing system, but also acts as a hole-transfer layer to facilitate the transfer of photogenerated holes from $CsPbBr_3$ to GDY, thus suppressing the electron−hole recombination. Furthermore, benefiting from the high loading capacity of metal ions, the GDY layer can serve as a compatible platform for decorating Co^{2+} to catalyze the reduction of CO_2. After doping of Co ions, the photocatalytic activity of $CsPbBr_3$@$GDY_{0.3}$-Co for the CO_2-to-CO conversion reaches up to 27.7 μmol g^{-1} h^{-1}, which is almost 8 times higher than that of pure $CsPbBr_3$. The GDY-protected $CsPbBr_3$, suppressed electron−hole recombination, doped Co active sites, and improved chemisorption of CO_2 on GDY are responsible for the enhancement of photocatalytic CO_2-to-CO reduction. This work provides a fascinating strategy for improving the stability and activity of metal-halide perovskite nanocrystals and broadens their applications in the field of energy conversion.

4. EXPERIMENTAL SECTION

4.1. Synthesis of $CsPbBr_3$@GDY. First, hexakis[(trimethylsilyl)-ethynyl]benzene (HEB-TMS) (1 mg, 3 mg, or 5 mg) was dissolved in tetrahydrofuran (5 mL) in a three-necked flask under Ar atmosphere at 273 K in the dark, followed by the quick addition of tetra-*n*-butylammonium fluoride (TBAF) (20 μL, 60 or 100 μL) into the above solution, after stirring for 10 min, hexakis(ethynyl)benzene (HEB) (0.33 mg, 0.99 mg, or 1.65 mg) was obtained by extraction operation. Second, the obtained HEB was dissolved in a mixed solvent of toluene and *n*-hexane (1:1, *v*:*v*) for use. Then, the as-prepared $CsPbBr_3$ (10 mg, see details in the SI) was added to the above solutions, and the reaction system was transferred to a microwave synthesizer and subjected to microwave irradiation for 10 min. Finally, the synthesized samples were washed, dried, and then stored in a vacuum desiccator for use. $CsPbBr_3$@GDY with different compound ratios were labeled as $CsPbBr_3$@$GDY_{0.1}$, $CsPbBr_3$@$GDY_{0.3}$, and $CsPbBr_3$@$GDY_{0.5}$, respectively.

4.2. Synthesis of $CsPbBr_3$@$GDY_{0.3}$-Co. The synthesis process of $CsPbBr_3$@$GDY_{0.3}$-Co is similar to that of $CsPbBr_3$@$GDY_{0.3}$, except that $CoBr_2$ (1 mg) and $CsPbBr_3$ (10 mg) were added to HEB mixture solution at the same time.

■ ASSOCIATED CONTENT

Supporting Information

The Supporting Information is available free of charge at https://pubs.acs.org/doi/10.1021/acsami.0c14826.

Preparation process of $CsPbBr_3$; the characterization of $CsPbBr_3$, $CsPbBr_3$@GDY, and $CsPbBr_3$@GDY-Co; and additional results of TEM, Raman spectra, XRD spectra, GC−MS analysis, UV−vis spectrum, Mott−Schottky plots, and XPS measurements (PDF)

■ AUTHOR INFORMATION

Corresponding Authors

Wen Zhang − *MOE International Joint Laboratory of Materials Microstructure, Institute for New Energy Materials and Low Carbon Technologies, School of Materials Science and Engineering, Tianjin University of Technology, Tianjin 300384, P. R. China;* orcid.org/0000-0001-6105-3286; Email: zhangwen@email.tjut.edu.cn

Min Zhang − *MOE International Joint Laboratory of Materials Microstructure, Institute for New Energy Materials and Low Carbon Technologies, School of Materials Science and Engineering and Tianjin Key Laboratory of Organic Solar Cells and Photochemical Conversion, School of Chemistry and Chemical Engineering, Tianjin University of Technology, Tianjin 300384, P. R. China;* orcid.org/0000-0002-0275-9497; Email: zm2016@email.tjut.edu.cn

Tong-Bu Lu − *MOE International Joint Laboratory of Materials Microstructure, Institute for New Energy Materials and Low Carbon Technologies, School of Materials Science and Engineering, Tianjin University of Technology, Tianjin 300384, P. R. China;* orcid.org/0000-0002-6087-4880; Email: lutongbu@tjut.edu.cn

Authors

Ke Su − *MOE International Joint Laboratory of Materials Microstructure, Institute for New Energy Materials and Low Carbon Technologies, School of Materials Science and Engineering, Tianjin University of Technology, Tianjin 300384, P. R. China*

Guang-Xing Dong − *MOE International Joint Laboratory of Materials Microstructure, Institute for New Energy Materials and Low Carbon Technologies, School of Materials Science and Engineering, Tianjin University of Technology, Tianjin 300384, P. R. China*

Zhao-Lei Liu − *MOE International Joint Laboratory of Materials Microstructure, Institute for New Energy Materials and Low Carbon Technologies, School of Materials Science and Engineering, Tianjin University of Technology, Tianjin 300384, P. R. China*

Complete contact information is available at: https://pubs.acs.org/10.1021/acsami.0c14826

Notes

The authors declare no competing financial interest.

https://dx.doi.org/10.1021/acsami.0c14826
ACS Appl. Mater. Interfaces 2020, 12, 50464−50471

■ ACKNOWLEDGMENTS

This work was financially supported by National Key R&D Program of China (2017YFA0700104), Natural Science Foundation of Tianjin City (17JCJQJC43800), NSFC (21790052 and 21702146), and the 111 Project of China (D17003).

■ REFERENCES

(1) Montoya, J. H.; Seitz, L. C.; Chakthranont, P.; Vojvodic, A.; Jaramillo, T. F.; Nørskov, J. K. Materials for Solar Fuels and Chemicals. *Nat. Mater.* **2017**, *16*, 70−81.
(2) Li, C.; Xu, Y.; Tu, W.; Chen, G.; Xu, R. Metal-Free Photocatalysts for Various Applications in Energy Conversion and Environmental Purification. *Green Chem.* **2017**, *19*, 882−899.
(3) Grills, D. C.; Ertem, M. Z.; Mckinnon, M.; Ngo, K. T.; Rochford, J. Mechanistic Aspects of CO_2 Reduction Catalysis with Manganese-Based Molecular Catalysts. *Coord. Chem. Rev.* **2018**, *374*, 173−217.
(4) Takeda, H.; Cometto, C.; Ishitani, O.; Robert, M. Electrons, Photons, Protons and Earth-Abundant Metal Complexes for Molecular Catalysis of CO_2 Reduction. *ACS Catal.* **2017**, *7*, 70−88.
(5) Pellegrin, Y.; Odobel, F. Sacrificial Electron Donor Reagents for Solar Fuel Production. *C. R. Chim.* **2017**, *20*, 283−295.
(6) Kärkäs, M. D.; Verho, O.; Johnston, E. V.; Åkermark, B. Artificial Photosynthesis: Molecular Systems for Catalytic Water Oxidation. *Chem. Rev.* **2014**, *114*, 11863−12001.
(7) Kovalenko, M. V.; Protesescu, L.; Bodnarchuk, M. I. Properties and Potential Optoelectronic Applications of Lead Halide Perovskite Nanocrystals. *Science* **2017**, *358*, 745−750.
(8) Li, X.; Cao, F.; Yu, D.; Chen, J.; Sun, Z.; Shen, Y.; Zhu, Y.; Wang, L.; Wei, Y.; Wu, Y.; Zeng, H. All Inorganic Halide Perovskites Nanosystem: Synthesis, Structural Features, Optical Properties and Optoelectronic Applications. *Small* **2017**, *13*, 1603996.
(9) Akkerman, Q. A.; Rainò, G.; Kovalenko, M. V.; Manna, L. Genesis, Challenges and Opportunities for Colloidal Lead Halide Perovskite Nanocrystals. *Nat. Mater.* **2018**, *17*, 394−405.
(10) Mu, Y.-F.; Zhang, W.; Dong, G.-X.; Su, K.; Zhang, M.; Lu, T.-B. Ultrathin and Small-Size Graphene Oxide as an Electron Mediator for Perovskite-Based Z-Scheme System to Significantly Enhance Photocatalytic CO_2 Reduction. *Small* **2020**, *16*, 2002140.
(11) Jiang, Y.; Liao, J.-F.; Chen, H.-Y.; Zhang, H.-H.; Li, J.-Y.; Wang, X.-D.; Kuang, D.-B. All-Solid-State Z-Scheme α-Fe_2O_3/Amine-RGO/$CsPbBr_3$ Hybrids for Visible-Light-Driven Photocatalytic CO_2 Reduction. *Chem.* **2020**, *6*, 766−780.
(12) Wang, J.; Wang, J.; Li, N.; Du, X.; Ma, J.; He, C.; Li, Z. Direct Z-Scheme 0D/2D Heterojunction of $CsPbBr_3$ Quantum Dots/Bi_2WO_6 Nanosheets for Efficient Photocatalytic CO_2 Reduction. *ACS Appl. Mater. Interfaces* **2020**, *12*, 31477−31485.
(13) Mu, Y.-F.; Zhang, W.; Guo, X.-X.; Dong, G.-X.; Zhang, M.; Lu, T.-B. Water-Tolerant Lead Halide Perovskite Nanocrystals as Efficient Photocatalysts for Visible-Light-Driven CO_2 Reduction in Pure Water. *ChemSusChem* **2019**, *12*, 4769−4774.
(14) Kong, Z.-C.; Liao, J.-F.; Dong, Y.-J.; Xu, Y.-F.; Chen, H.-Y.; Kuang, D.-B.; Su, C.-Y. Core@Shell $CsPbBr_3$@Zeolitic Imidazolate Framework Nanocomposite for Efficient Photocatalytic CO_2 Reduction. *ACS Energy Lett.* **2018**, *3*, 2656−2662.
(15) Hou, J.; Cao, S.; Wu, Y.; Gao, Z.; Liang, F.; Sun, Y.; Lin, Z.; Sun, L. Inorganic Colloidal Perovskite Quantum Dots for Robust Solar CO_2 Reduction. *Chem. - Eur. J.* **2017**, *23*, 9481−9485.
(16) Chen, J.; Dong, C.; Idriss, H.; Mohammed, O. F.; Bakr, O. M. Metal Halide Perovskites for Solar-to-Chemical Fuel Conversion. *Adv. Energy Mater.* **2020**, *10*, 1902433.
(17) Huang, H.; Pradhan, B.; Hofkens, J.; Roeffaers, M. B. J.; Steele, J. A. Solar-Driven Metal Halide Perovskite Photocatalysis: Design, Stability, and Performance. *ACS Energy Lett.* **2020**, *5*, 1107−1123.
(18) Chen, P.; Ong, W.-J.; Shi, Z.; Zhao, X.; Li, N. Pb-Based Halide Perovskites: Recent Advances in Photo(electro)catalytic Applications and Looking Beyond. *Adv. Funct. Mater.* **2020**, *30*, 1909667.
(19) Wu, H.; Li, X.-B.; Tung, C.-H.; Wu, L.-Z. Semiconductor Quantum Dots: An Emerging Candidate for CO_2 Photoreduction. *Adv. Mater.* **2019**, *31*, 1900709.
(20) Wei, Y.; Cheng, Z.; Lin, J. An Overview on Enhancing the Stability of Lead Halide Perovskite Quantum Dots and Their Applications in Phosphor-Converted LEDs. *Chem. Soc. Rev.* **2019**, *48*, 310−350.
(21) Cho, H.; Kim, Y. H.; Wolf, C.; Lee, H. D.; Lee, T. W. Improving the Stability of Metal Halide Perovskite Materials and Light-Emitting Diodes. *Adv. Mater.* **2018**, *30*, 1704587.
(22) Huang, H.; Bodnarchuk, M. I.; Kershaw, S. V.; Kovalenko, M. V.; Rogach, A. L. Lead Halide Perovskite Nanocrystals in the Research Spotlight: Stability and Defect Tolerance. *ACS Energy Lett.* **2017**, *2*, 2071−2083.
(23) Xu, Y.-F.; Yang, M.-Z.; Chen, B.-X.; Wang, X.-D.; Chen, H.-Y.; Kuang, D.-B.; Su, C.-Y. A $CsPbBr_3$ Perovskite Quantum Dot/Graphene Oxide Composite for Photocatalytic CO_2 Reduction. *J. Am. Chem. Soc.* **2017**, *139*, 5660−5663.
(24) Ou, M.; Tu, W.; Yin, S.; Xing, W.; Wu, S.; Wang, H.; Wan, S.; Zhong, Q.; Xu, R. Amino-Assisted Anchoring of $CsPbBr_3$ Perovskite Quantum Dots on Porous g-C_3N_4 for Enhanced Photocatalytic CO_2 Reduction. *Angew. Chem., Int. Ed.* **2018**, *57*, 13570−13574.
(25) Wu, L.-Y.; Mu, Y.-F.; Guo, X.-X.; Zhang, W.; Zhang, Z.-M.; Zhang, M.; Lu, T.-B. Encapsulating Perovskite Quantum Dots in Iron-Based Metal−Organic Frameworks (MOFs) for Efficient Photocatalytic CO_2 Reduction. *Angew. Chem., Int. Ed.* **2019**, *58*, 9491−9495.
(26) Shyamal, S.; Dutta, S. K.; Pradhan, N. Doping Iron in $CsPbBr_3$ Perovskite Nanocrystals for Efficient and Product Selective CO_2 Reduction. *J. Phys. Chem. Lett.* **2019**, *10*, 7965−7969.
(27) Chen, Z.; Hu, Y.; Wang, J.; Shen, Q.; Zhang, Y.; Ding, C.; Bai, Y.; Jiang, G.; Li, Z.; Gaponik, N. Boosting Photocatalytic CO_2 Reduction on $CsPbBr_3$ Perovskite Nanocrystals by Immobilizing Metal Complexes. *Chem. Mater.* **2020**, *32*, 1517−1525.
(28) Zhu, J.; Zhu, Y.; Huang, J.; Hou, L.; Shen, J.; Li, C. Synthesis of Monodisperse Water-Stable Surface Pb-Rich $CsPbCl_3$ Nanocrystals for Efficient Photocatalytic CO_2 Reduction. *Nanoscale* **2020**, *12*, 11842−11846.
(29) Li, G.; Li, Y.; Liu, H.; Guo, Y.; Li, Y.; Zhu, D. Architecture of Graphdiyne Nanoscale Films. *Chem. Commun.* **2010**, *46*, 3256−3258.
(30) Yin, C.; Li, J.; Li, T.; Yu, Y.; Kong, Y.; Gao, P.; Peng, H.; Tong, L.; Zhang, J. Catalyst-Free Synthesis of Few-Layer Graphdiyne Using a Microwave-Induced Temperature Gradient at a Solid/Liquid Interface. *Adv. Funct. Mater.* **2020**, *30*, 2001396.
(31) Wang, F.; Zuo, Z.; Li, L.; He, F.; Lu, F.; Li, Y. A Universal Strategy for Constructing Seamless Graphdiyne on Metal Oxides to Stabilize the Electrochemical Structure and Interface. *Adv. Mater.* **2018**, *31*, 1806272.
(32) Lin, Z.-Z. Graphdiyne as a Promising Substrate for Stabilizing Pt Nanoparticle Catalyst. *Carbon* **2015**, *86*, 301−309.
(33) Shekar, S. C.; Swathi, R. S. Cation-π Interactions and Rattling Motion through Two-Dimensional Carbon Networks: Graphene vs Graphynes. *J. Phys. Chem. C* **2015**, *119*, 8912−8923.
(34) Li, J.; Gao, X.; Liu, B.; Feng, Q.; Li, X.-B.; Huang, M.-Y.; Liu, Z.; Zhang, J.; Tung, C.-H.; Wu, L.-Z. Graphdiyne: A Metal-Free Material as Hole Transfer Layer to Fabricate Quantum Dot-Sensitized Photocathodes for Hydrogen Production. *J. Am. Chem. Soc.* **2016**, *138*, 3954−3957.
(35) Ihm, K.; Kang, T.-H.; Lee, D. H.; Park, S.-Y.; Kim, K.-J.; Kim, B.; Yang, J. H.; Park, C. Y. Oxygen Contaminants Affecting on the Electronic Structures of the Carbon Nano Tubes Grown by Rapid Thermal Chemical Vapor Deposition. *Surf. Sci.* **2006**, *600*, 3729−3733.
(36) Estrade-Szwarckopf, H. XPS Photoemission in Carbonaceous Materials: A "Defect" Peak Beside the Graphitic Asymmetric Peak. *Carbon* **2004**, *42*, 1713−1721.
(37) Rao, H.; Schmidt, L. C.; Bonin, J.; Robert, M. Visible-Light-Driven Methane Formation from CO_2 with a Molecular Iron Catalyst. *Nature* **2017**, *548*, 74−77.

https://dx.doi.org/10.1021/acsami.0c14826
ACS Appl. Mater. Interfaces 2020, 12, 50464−50471

(38) Huang, C. S.; Li, Y. J.; Wang, N.; Xue, Y. R.; Zuo, Z. C.; Liu, H. B.; Li, Y. L. Progress in Research into 2D Graphdiyne-Based Materials. *Chem. Rev.* **2018**, *118*, 7744−7803.
(39) Li, J.; Gao, X.; Liu, B.; Feng, Q. L.; Li, X. B.; Huang, M. Y.; Liu, Z. F.; Zhang, J.; Tung, C. H.; Wu, L. Z. Graphdiyne: A Metal-Free Material as Hole Transfer Layer To Fabricate Quantum Dot-Sensitized Photocathodes for Hydrogen Production. *J. Am. Chem. Soc.* **2016**, *138*, 3954−3957.
(40) Han, Y. Y.; Lu, X. L.; Tang, S. F.; Yin, X. P.; Wei, Z. W.; Lu, T. B. Metal-Free 2D/2D Heterojunction of Graphitic Carbon Nitride/Graphdiyne for Improving the Hole Mobility of Graphitic Carbon Nitride. *Adv. Energy Mater.* **2018**, *8*, 1702992.
(41) Lv, J.-X.; Zhang, Z.-M.; Wang, J.; Lu, X.-L.; Zhang, W.; Lu, T.-B. In Situ Synthesis of CdS/Graphdiyne Heterojunction for Enhanced Photocatalytic Activity of Hydrogen Production. *ACS Appl. Mater. Interfaces* **2019**, *11*, 2655−2661.
(42) Cao, S.; Wang, Y.; Zhu, B.; Xie, G.; Yu, J.; Gong, J. R. Enhanced Photochemical CO_2 Reduction in the Gas Phase by Graphdiyne. *J. Mater. Chem. A* **2020**, *8*, 7671−7676.
(43) Wu, B.; Li, M.; Xiao, S.; Qu, Y.; Qiu, X.; Liu, T.; Tian, F.; Li, H.; Xiao, S. A Graphyne-Like Porous Carbon-Rich Network Synthesized via Alkyne Metathesis. *Nanoscale* **2017**, *9*, 11939−11943.
(44) Yin, X.-P.; Wang, H.-J.; Tang, S.-F.; Lu, X.-L.; Shu, M.; Si, R.; Lu, T.-B. Engineering the Coordination Environment of Single-Atom Platinum Anchored on Graphdiyne for Optimizing Electrocatalytic Hydrogen Evolution. *Angew. Chem., Int. Ed.* **2018**, *57*, 9382−9386.
(45) Xue, Y.; Huang, B.; Yi, Y.; Guo, Y.; Zuo, Z.; Li, Y.; Jia, Z.; Liu, H.; Li, Y. Anchoring Zero Valence Single Atoms of Nickel and Iron on Graphdiyne for Hydrogen Evolution. *Nat. Commun.* **2018**, *9*, 1460.
(46) Qi, H.; Yu, P.; Wang, Y.; Han, G.; Liu, H.; Yi, Y.; Li, Y.; Mao, L. Graphdiyne Oxides as Excellent Substrate for Electroless Deposition of Pd Clusters with High Catalytic Activity. *J. Am. Chem. Soc.* **2015**, *137*, 5260−5263.
(47) Zhu, H.; Zhang, J.; Yanzhang, R.; Du, M.; Wang, Q.; Gao, G.; Wu, J.; Wu, G.; Zhang, M.; Liu, B.; Yao, J.; Zhang, X. When Cubic Cobalt Sulfide Meets Layered Molybdenum Disulfide: A Core-Shell System toward Synergetic Electrocatalytic Water Splitting. *Adv. Mater.* **2015**, *27*, 4752−4759.
(48) Wu, W. Q.; Ding, K. L.; Liu, J.; Drake, T.; Stair, P.; Weitz, E. Methanol Oxidation to Formate on ALD-Prepared VO_x/θ-Al_2O_3 Catalysts: A Mechanistic Study. *J. Phys. Chem. C* **2017**, *121*, 26794−26805.
(49) Lu, Z. K.; Gao, Y.; Chen, H.; Liu, Z.; Chen, L. F.; Sun, L. C. Efficient molecular ruthenium catalysts containing anionic ligands for water oxidation. *Dalton Trans* **2016**, *45*, 18459−18464.

https://dx.doi.org/10.1021/acsami.0c14826
ACS Appl. Mater. Interfaces 2020, 12, 50464−50471